Exploring the physicochemical and antimicrobial properties of gold-chitosan hybrid nanoparticles composed of varying chitosan amounts.

Mohamed A. Mohamady Hussein [a,b,]∗, F. Guillermo Díaz Baños [c], Mariusz Grinholc [d], Ahmed S. Abo Dena [e], Ibrahim M. El-Sherbiny [e], Mosaad Megahed [a]

[a] Clinic of Dermatology, University Hospital of Aachen, Aachen 52074, Germany [b] Department of Pharmacology, Medical Research Division, National Research Center, Dokki 12622, Cairo, Egypt [c] Department of Physical Chemistry, University of Murcia, Murcia 30100, Spain [d] Laboratory of Molecular Diagnostics, Department of Biotechnology, Intercollegiate Faculty of Biotechnology, University of Gdansk, Gdansk, Poland [e] Nanomedicine Laboratory, Center for Materials Science (CMS), Zewail City of Science and Technology, 6th of October, Giza 12578, Egypt

∗ Corresponding author. E-mail address: almohammadeymr2023@gmail.com (M.A. Mohamady Hussein).

Abstract

A green synthesis method for gold-chitosan hybrid nanoparticles (Au-CS hNPs) using different concentrations of CS as a capping/reducing agent is reported to investigate the effect of CS concentration on the physicochemical properties as well as the antimicrobial activity of the developed Au-CS hNPs. The as-synthesized Au-CS hNPs were characterized using visible spectrophotometry, FTIR, dynamic light scattering, DSC, XRD, SEM-EDX and TEM. The size of the formed hNPs ranges from 16.9 ± 3.9 nm (highest CS concentration) to 34.7 ± 7.6 nm (lowest CS concentration). It was noticed that increasing the amount of CS increases the ζ-potential from +25.1 to +53.1 mV and enhances the 6-months stability of the produced Au-CS hNPs. Furthermore, the obtained results indicated that the antimicrobial activity, in terms of MIC and CFU assays, is directly proportional to the amount of CS used in the preparation procedure. FTIR analysis revealed that the mechanism of formation of the Au-CS hNPs may involve complexation of CS with Au ions via its NH_2 and OH groups followed by the chemical reduction of Au ions to metallic Au NPs. Eventually, higher amounts of CS are necessary for synthesizing highly stable Au-CS hNPs with small size, homogeneous shape and potent antibacterial/antifungal properties.

1. Introduction

For many years, nanotechnology (the engineering of functional systems at the nanoscale) has been the interest of scientists because it provides solutions for many challenges in various fields such as medicine, pharmacy, optics, electronics and agriculture as well as in energy production and storage. Besides, the ability to construct intricate, large structures with nanometer precision is rapidly progressing and includes bottom-up additive approaches and top-down reductive approaches [1]. However, most of these fabrication methods require the use of hazardous chemicals which constitute an obstacle for scaling up purposes.

Amongst the nanomaterials that displayed promising characteristics suitable for a wide range of applications are gold nanoparticles (Au NPs) as they were successfully applied in optics, electronics, sensing, biomedicine, catalysis, etc. The unique properties of Au NPs include being nontoxic, non-immunogenic, highly stable, easy to prepare with different particle sizes (2–500 nm) and shapes, susceptible to surface modifications as well as being with distinctive optical and electronic properties. Despite having all these advantages, the low efficiency of Au NPs as antimicrobial agents is still challenging where surface functionalization and hybridization with other materials can provide solutions for such pitfalls. Fortunately, Au NPs offer a large surface area which can be coated with different therapeutic agents in order to increase their antimicrobial potency against resistant microorganisms [2].

Chitosan (CS), a natural aminated polysaccharide extracted from crustaceans' shells and fungal cell walls, is a biocompatible, watersoluble and biodegradable polymer [3,4]. Possessing reactive NH_2 and OH functional groups allows CS to be easily functionalized and to be used as a reducing and capping agent for synthesizing metal nanoparticles (NPs). The literature is flooded of the methods of synthesis of metal/ CS NPs [5–7]. The most common method applied for obtaining Au NPs involves the chemical reduction of ionic gold (obtained from gold III chloride trihydrate) into metallic gold using chemical reducing agents

such as sodium borohydrate (NaBH$_4$) in the presence of appropriate stabilizing agents [8]. Employing naturally occurring polymers and/or plant and microorganisms extracts as reducing agents, capping agents and stabilizers for Au NPs grasped the attention of researchers for various applications including diagnostics [9], anti-inflammation [10], biomarkers [11], insulin delivery [12], anti-bacterial infections [13] and cancer treatments [11,14]. Mohan et al. prepared CS-capped Au NPs via using CS as both capping and reducing agent, followed by investigating the ability of the developed CS-capped Au NPs to indicate any temperature abuse in frozen products [15]. Reicha et al. prepared Ag/CS hybrid NPs by applying an electrochemical oxidation step of Ag ions, followed by chemical reduction by CS [6]. They reported that the mechanism of formation of Ag/CS hybrid NPs involves a complexation step (the formation of CS-Ag complex) prior to the chemical reduction of silver ions.

In the present work, a series of gold/chitosan hybrid nanoparticles (Au-CS hNPs) was synthesized via a green method using different concentrations of CS as a capping and reducing agent. The main objective of the study was to investigate the influence of CS concentration on the physicochemical properties (particle size, shape, surface charge, thermal stability, crystallinity, etc.) as well as the antimicrobial activities of the synthesized Au-CS hNPs with the aid of different characterization and microbiological analyses. Moreover, an anticipated mechanism for the formation of the Au-CS hNPs at the molecular level was proposed.

2. Materials and methods

2.1. Materials

CS of a molecular weight of 45 kDa and degree of acetylation around 80% was purchased from Sigma-Aldrich, UK (448877-250G). Glacial acetic acid and HAuCl$_4$·3H$_2$O (99.5%) were obtained from Panreac and Sigma Aldrich (Germany), respectively. Ultrapure milli-Q water was used for all solutions preparation.

2.2. Microorganism strains

Reference microbial strains included Staphylococcus aureus Newman, Pseudomonas aeruginosa ATCC 10145, and Candida albicans ATCC 2091. The microbes were grown overnight in trypticase soy broth (TSB) (bioMérieux) medium at 37 °C while shaking at 150 rpm.

2.3. Preparation of Au-CS hybrid nanoparticles

CS stock solution was prepared by adding CS powder to an aqueous acetic acid solution (1%, w/v) and the suspension was stirred overnight until a clear solution was obtained. The resulting CS stock solution was then diluted with milli-Q water at pH 3.5–4 to the required concentrations (1.00, 0.50, 0.25, 0.10 and 0.05 mg/mL). Afterwards, 50 mL of the CS solution was taken, stirred at 750 rpm and heated up to 80 °C. Thereafter, 50 µL of AuHCl$_4$ (125 mmol/L) was added to the solution and left for 15 min. The synthesized Au-CS hNPs were denoted NP1, NP2, NP3, NP4 and NP5 upon using 50, 100, 250, 500 and 1000 µg/mL of CS, respectively. The transformation of the clear solutions to wine red color was taken as a preliminary indication for the formation of the NPs. The resulting Au-CS hNPs were collected by ultracentrifugation at 28,000rpm at 25 °C for 30min. The supernatants recovered from centrifugation were discarded and the pellets were re-suspended in milli-Q water and characterized.

2.4. Characterization of the Au-CS nanoparticles

Visible electronic absorption spectra of the developed Au-CS hNPs were recorded using a T92+ double-beam UV–Vis Spectrophotometer (PG Instruments, UK) over the range 400–800 nm. Particle size and zeta potential (ζ) measurements were carried out by dynamic light scattering (DLS) using a Malvern Zetasizer Nano ZS (Malvern Instruments Ltd., UK). DLS measurements were carried out at 633 nm. Particle size was determined by considering that the particles have a spherical shape. Using photodiode detector, the scattering intensity was measured at a 173° angle relative to the source (backscattering). Each sample was measured three times and each measurement was run ten times of 10 s each. Size and morphology of Au-CS hNPs were investigated with TEM (JEOL TEM-1011) attached to a Gatan Bioscan Camera model 792 for imaging acquisition at accelerating voltage of 100 kV. TEM samples were prepared by depositing 10 µL of the colloidal suspensions on a 200 mesh formvar/carbon film-coated Cu/Ni grid, followed by air-drying. Excess film was removed with absorbent paper. Histograms of the NPs size distribution were generated with ImageJ®. The microstructure of the Au-CS NPs was also examined using a scanning electron microscope (Philips XL 30 SEM) coupled with an energy-dispersive Xray (EDX) unit, operated at accelerating voltage of 25 kV. All infrared measurements were performed using a Mattson 5000 FTIR spectrometer at 25 °C in the range of 4000–4000 cm^{-1} at a resolution of 8 cm^{-1}. A drop of diluted Au-CS NPs samples was spread onto planar freshly cleaved sodium chloride disks. The solvent was completely pumped out at a temperature of 50 °C, and then the disks were placed in the sample holder of the spectrometer. The X-ray diffraction (XRD) patterns of the selected Au-CS hNPs samples were obtained using Philips PW 1390 X-ray diffractometer. X-rays were provided with a beam monochromator and Cu Kα radiation at $\lambda = 1.54$ Å. The applied voltage was 40 kV and the current intensity was 40 mA s. The 2θ angle was recorded in the range of 10–80° with a scanning speed of 2°/min. The crystallinity of the developed samples was also calculated with the aid of Material Studio Vision (MSV) software, version 4.4. A differential scanning calorimeter (DSC) was used for thermal analysis measurements.

2.5. Assessment of the antimicrobial activity

2.5.1. Minimal inhibitory concentration

The NPs powder was accurately weighed and added to distilled water or 0.25% acetic acid to make a 1 mg/mL solution. The minimum inhibitory concentration (MIC) was determined by a broth dilution method performed in 96-well microtiter plates. The bacterial concentration was standardized using the McFarland scale to (approximately 1.5×10^7 CFU/mL) Muller-Hinton (MH) Broth. Thereafter, 100 µL of inoculants were mixed with 100 µL of two-fold serial dilutions of different treatment groups and were subsequently incubated at 37 °C for 20 h. The lowest concentration that completely inhibits visual growth of bacteria (no turbidity) was considered as the MIC.

2.5.2. CFU assay

Microbial overnight cultures were adjusted to an optical density (OD) of 0.5 McFarland (McF) (10^7 CFU/mL) for S. aureus and P. aeruginosa, meanwhile C. albicans cultures were adjusted to OD of 5

McFarland (McF) (10^6 CFU/mL). The cells were then transferred to a 96-well microtiter plate (100 μL per well). The developed hNPs were then added to the bacterial suspensions at concentration of 7.8 up to 500 mg/mL. Aliquots of 10 μL were obtained from wells with no visible bacterial growth in order to determine the CFU values. The contents of the wells were mixed before sampling, and the aliquots were serially diluted (10 folds) in phosphate buffer saline (PBS) (0.13 mmol/L NaCl, 8.1 mmol/L Na_2HPO_4, 2.68 mmol/L KCl and 1.47 mmol/L KH_2PO_4) to achieve final dilutions of 10^{-1} to 10^{-6}, which were then streaked horizontally as previously reported [16]. Each experiment was carried out in triplicate (i.e. three independent experiments with three repetitions per sample; the time interval between the three replicates was 24 h). The survival fraction was expressed as the ratio of the CFU of bacteria treated with NPs or CS to the CFU of the untreated pathogen. For the purpose of this study, lethal doses of the tested samples were detected (as recommended elsewhere [17]) as the concentration that resulted in an approximately ≥3 $\log_{10}$ reduction in CFU. A sub-lethal dose could be considered as the concentration which produces a 2 $\log_{10}$ reduction in the survival of the microbial cells.

3. Results and discussion

3.1. Preparation of Au-CS hybrid nanoparticles

3.1.1. Surface plasmon resonance

The method used herein for the synthesis of Au-CS hNPs depends on the chemical reduction of gold ions into metallic Au NPs in the presence of CS as a capping and reducing agent. The reducing properties of CS are due to the possession of the reducing NH_2 and OH functional groups in its β(1-4) D-glucosamine units [6]. The influence of the capping agent on the formation of Au NPs in aqueous and non-aqueous media was studied by Lindhe et al. [18]. Therefore, it was expected that changing the amount of CS during the chemical synthesis of Au NPs may have a significant effect on the size, shape and antibacterial properties of the resulting Au-CS hNPs. The formation of Au-CS hNPs was confirmed with the aid of visible-light absorption spectrophotometry where obvious absorption bands were observed at about 529 nm (Fig. 1).

The electronic absorption spectra of free acidic CS solution as well as the Au-CS hNPs suspensions prepared with different CS concentrations were compared in order to investigate the effect of the amount of CS on the reduction rate of Au ions. Free CS solution showed no absorption bands over the entire visible region of the electromagnetic spectrum which agrees with the previously reported results. However, NP3, NP4 and NP5 solutions demonstrated a single absorption band at about 529 nm. It is worth to mention that NP1 and NP2 solutions showed a very week absorption band at the same position that disappeared after 1–2 days indicating that the first two CS concentrations used to prepare NP1 and NP2 were not sufficient for the complete reduction process. The disappearance of the NP1 and NP2 absorption band may be attributed to the flocculation of the small amount of large-sized Au-CS hNPs. The intensities of the absorption bands follow the order NP5 > NP4 > NP3, revealing that there is a direct relationship between the amount of the produced Au-CS hNPs and the used concentration of capping/reducing agent (i.e. CS). This might reflect the rate of chemical reduction of gold ions; so that, one can say that the rate of chemical reduction of gold ions is directly proportional to the used amount of CS as a capping/reducing agent. An acceptable

explanation for these results could be that the amount of available free NH_2 and OH groups is higher in case of high concentrations of CS.
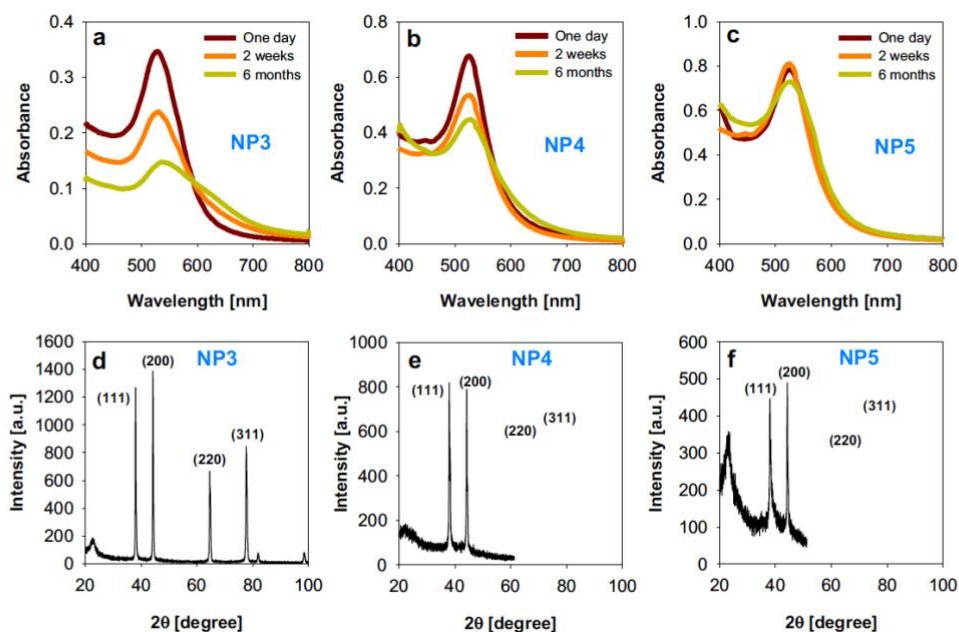

Fig. 1. Visible electronic absorption bands of Au-CS hNPs at different time intervals from the day of preparation up to 6 months (a–c). Panels (d–f) depict the X-ray diffraction patterns of Au–Cs hNPs.

Visible light absorption spectrophotometry was also used to assess the stability of the as-produced Au-CS hNPs by recording the electronic absorption spectra of the NPs solutions two weeks and six months after preparation. It was found that increasing the amount of CS stabilizes the produced Au-CS hNPs (Fig. 1). The intensity of the absorption band decreases by time in case of NP3 and NP4, yet it remains almost constant in case of NP5 suspension which contains the highest amount of CS. The absorption band of NP3 became broader and shifted to longer wavelengths, 532 and 536 nm after 2 weeks and 6 months of preparation, respectively. On the other hand, NP5 showed almost no broadening and a very slight blue shift (~526 nm) within 6 months after preparation. The observed blue shift reflects the band gap increase because of the quantum confinement effect [19].

3.1.2. X-ray diffraction

The formation and structures of the Au-CS hNPs synthesized with different concentrations of the capping/reducing agent (CS) were investigated using XRD analysis. XRD patterns with 2θ values ranging from 20° to 100° depict four diffraction peaks at 38.1, 44.2, 64.6 and 77.6 corresponding to the standard Bragg diffractions from the (111), (200), (220) and (311) planes of the face-centered cubic gold crystal structure (Fig. 1) [20]. The average crystallite size was calculated from the full width at half maximum (FWHM) of the diffraction peak corresponding to the (220) diffraction plane by using the Debye-Scherrer formula represented by Eq. (1) [21].

$$D = K\lambda = \beta \cos \theta \qquad (1)$$

where D is the crystallite size, K is the Scherrer's constant (K = 0.94), β corresponds to the FWHM of the selected XRD peak expressed in radians, and θ is the selected diffraction peak position. The calculated

average crystallite size was 3.55, 4.01 and 4.16 nm for NP3, NP4 and NP5, respectively. Based on the above XRD results, the formation of Au-CS hNPs was confirmed by the obtained diffraction peaks that agree with those previously reported in the literature.
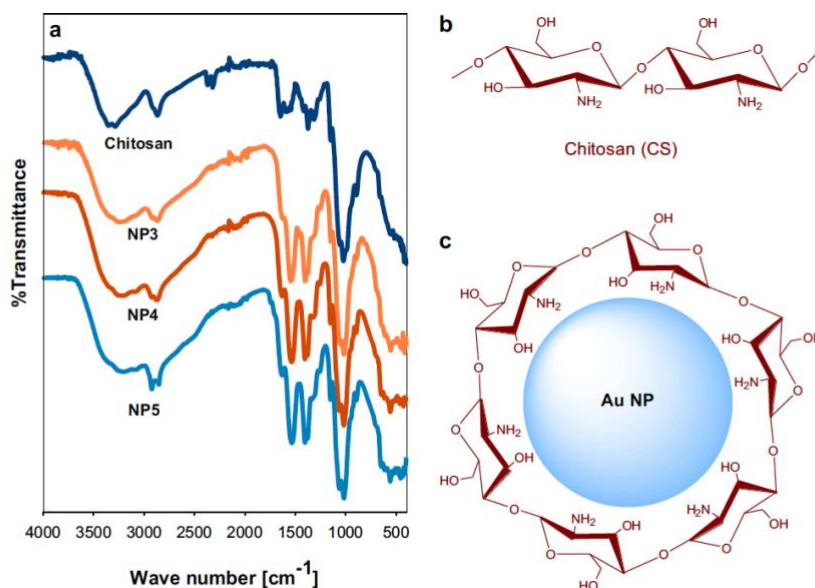

Fig. 2. (a) FTIR spectra of CS, NP3, NP4 and NP5, (b) chemical structure of chitosan dimer, and (c) a schematic illustration representing the interactions of the amino and hydroxyl groups of CS with gold ions to form an Au-CS hNP.

3.2. FTIR spectroscopy

FTIR spectroscopy is a vital analytical tool in nanomaterials synthesis and characterization as it enables the detection of functional group interactions and the formation of the end products [22,23]. That is why it can help in understanding the solution chemistry of nanomaterials synthesis. In order to further elucidate the formation of the Au-CS hNPs as well as to unravel the interaction between CS and gold ions, FTIR spectra of free CS, NP3, NP4 and NP5 were recorded and compared.

The FTIR spectrum of CS is well known for its characteristic $N-H$ and $O-H$ stretching vibration bands at ca. 3200–3500 cm^{-1}. The absorption bands appearing at 1646, 1589 and 1375 cm^{-1} are characteristic for the amide I, II and III, respectively. $C-O$ stretching band appeared at 1315 cm^{-1} [24,25]. In the FTIR spectra of NP3, NP4 and NP5, the band appearing at 3300 cm^{-1} has been shifted to 3280, 3278 and 3266 cm^{-1}, respectively. The broadening of these CS bands after heating with the gold precursor for 5 min may be an evidence for the interaction of CS with gold ions during the synthesis of Au-CS hNPs. Moreover, the attachment of the amino groups of CS to the gold ions caused a shift in the band corresponding to $N-H$ bending from 1646 cm^{-1} to 1640, 1631 and 1631 cm^{-1} in the case of NP3, NP4 and NP5, respectively. In addition, the amide III absorption band was diminished and replaced with a new band that appeared at 1403 cm^{-1} in all Au-CS hNPs. It is worth to mention that the absorption band attributed to the free amino groups of CS appearing at 1024 cm^{-1} demonstrated a CSconcentration dependent shift. The new bands appeared at 1020, 1018 and 1016 cm^{-1} in NP3, NP4 and NP5, respectively. Previous studies reported the interaction of the amine/hydroxyl groups of CS with metal ions during the synthesis of nanomaterials which agrees with the findings obtained herein [15].
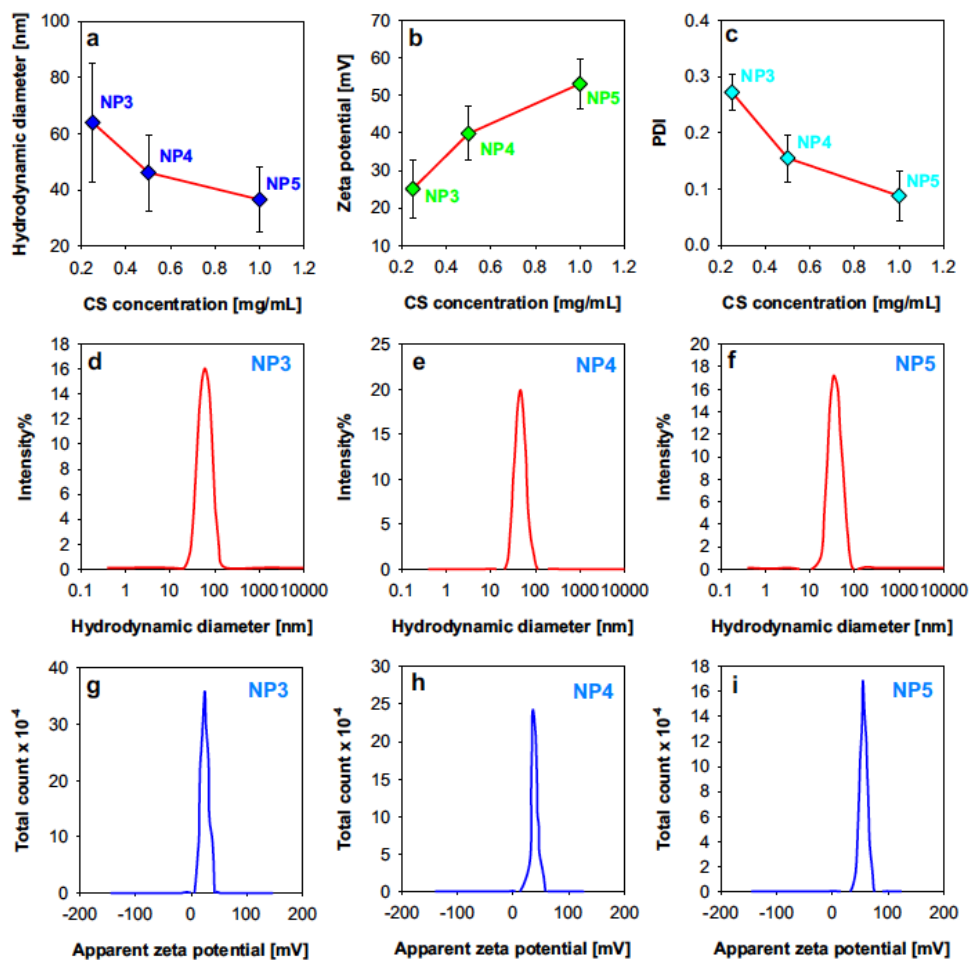
Fig. 3. Effect of CS concentration on (a) Au-CS hNPs size distribution, (b) ζ-potential, and (c) PDI. Panels (d–f) depict the size distribution of NP3, NP4 and NP5, respectively. Panels (g–i) show the apparent ζ-potential of NP3, NP4 and NP5, respectively.

Based on the above-discussed FTIR findings, the mechanism of formation of the as-synthesized Au-CS hNPs might involve a two-step process (Fig. 2). The first step includes the complexation of CS with gold ions via amino and hydroxyl groups. This step is followed by a chemical reduction step in which gold ions are converted into metallic Au NPs enclosed in a CS coating.

3.3. Nanoparticles size and ζ-potential

The particle size distribution and ζ-potential of the as-synthesized Au-CS hNPs were measured with dynamic light scattering (DLS). As shown in Fig. 3(a–c), increasing the amount of CS during the synthesis process leads to a significant decrease in particle size and polydispersity index (PDI), and an increase in the apparent ζ-potential (i.e. more positive potential). The particle size of NPs plays an important role in controlling their chemical, physical, optical and electronic properties. The mean particle size (hydrodynamic diameter) of the developed Au-CS hNPs were measured using DLS over the range of tested concentrations of CS (250, 500 and 1000 μg/mL) and the results are shown in Fig. 3. The plot of the mean hydrodynamic diameter exhibited a decrease in particle diameters with increasing CS concentration with NP5 demonstrating the smallest hydrodynamic diameter. This effect can be attributed to the availability of CS which induces the chemical reduction of gold ions and prevents the aggregation of the formed Au NPs via efficiently capping their surfaces. On the other hand, at low concentrations of CS, the reduction rate of

gold ions is slower and the amount of the capping agent is not enough for preventing the aggregation of the produced Au NPs resulting in a significant increase in size.
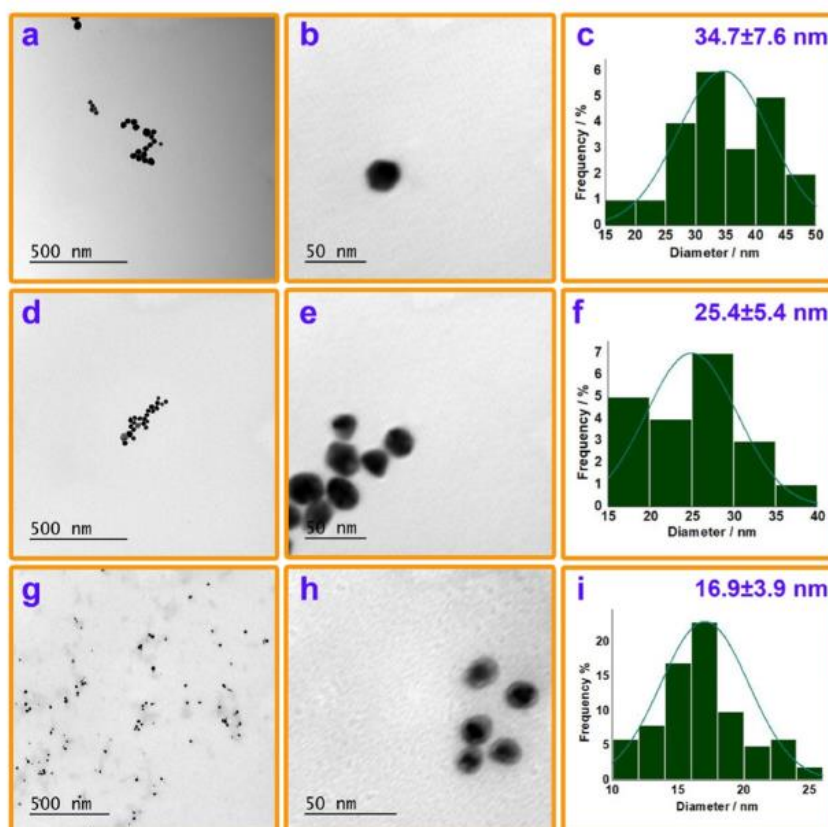

Fig. 4. TEM images and nanoparticle size distributions of NP3 (a–c), NP4 (d–f) and NP5 (g–i). The numbers on panels c, f and i resemble the average size of the Au-CS hNPs ±SD.

Zeta potential is a necessary parameter in the assessment of the stability of NPs in aqueous solutions. Particles with large negative/positive ζ-potentials tend to repel one another, and thereby are stable in aqueous solutions. However, in the case of low ζ-potential values attraction forces between the NPs dominate and, consequently the particles undergo flocculation and aggregation [21]. Generally speaking, a minimum ζ-potential of ±30 mV is necessary for stabilizing an aqueous suspension of NPs [21]. Fig. 3 shows the ζ-potential values of the asprepared Au-CS hNPs (+25.1, +39.8 and + 53.1 mV for NP3, NP4 and NP5, respectively) which indicate the high stability of the developed Au\\Cs hNPs due to the addition of positive charges from the CS coating. From these values, it is also apparent that the higher the concentration of CS, the higher is the stability of the formed Au-CS hNPs. This is consistent with the stability results obtained from the electronic absorbance spectra discussed above. In conclusion, NP5 showed the highest positive ζ-potential, and thereby its aqueous suspension attained the highest stability.

The size and shape of the as-synthesized Au-CS hNPs (NP3, NP4 and NP5) were investigated with the aid of TEM. The transmission electron micrographs depicted that the formed Au-CS hNPs are spherical with the smallest size (ca. 16.9 ± 3.9 nm) obtained upon using the highest concentration of CS (i.e. NP5). In addition, NP5 showed the narrowest size distribution. A strong Au-CS interaction could be clearly observed using high-resolution TEM at 50 nm magnification, particularly in the case of NP5 where a glory of CS is obvious around the central Au NPs (Fig. 4). Indeed, the particle size obtained from the TEM analysis is more accurate than the DLS analysis results which can be strongly affected by sedimentation of large particles and aggregates. Moreover, the size of the Au-CS hNPs obtained from the TEM imaging is

smaller than its DLS counterparts which might be attributed to the swelling of the CS organic coating on the outer surface of the Au NPs by the solvent used for sample preparation in DLS measurements [26].
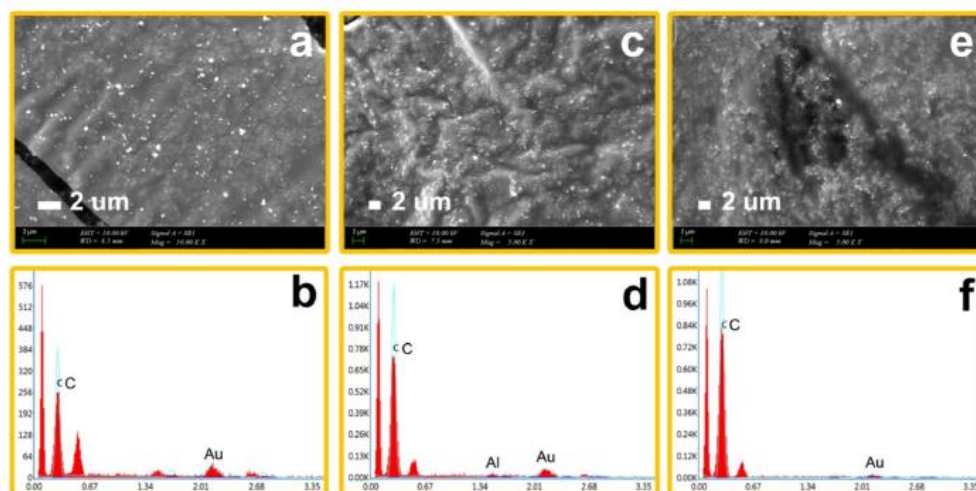

Fig. 5. SEM images (a, c and e) and EDX spectra (b, d and f) of Au-CS hNPs at different CS concentration: NP3 (a, b), NP4 (c, d) and NP5 (e, f).

3.4. Scanning electron microscopy (SEM)

The morphology of the synthesized Au-CS hNPs was examined with SEM. As can be noted from Fig. 5, the Au-CS hNPs appear as homogeneously-distributed spherical particles; however, NP3 demonstrated a slight aggregation.

Fig. 5 also shows the EDX analysis results of NP3, NP4 and NP5. The signal that appeared at ca. 2.3 keV indicates the presence of metallic crystalline Au NPs [27]. The intensities of the signals follow the order NP3 > NP4 > NP5 indicating that the thickness of the CS coating increases by increasing the CS concentration during the synthesis of AuCS hNPs. The SEM-EDX analysis revealed the presence of metallic Au NPs which is in a good agreement with the findings previously reported for the synthesis of Au NPs using Acanthopanacis cortex extract [28].

3.5. Differential scanning calorimetry (DSC)

The thermal behavior of CS and the developed Au-CS hNPs was studied with DSC over the temperature range 30–450 °C (Fig. 6). The pure CS powder showed a broad endothermic peak at 65–115 °C which can be attributed to dehydration. On the other hand, NP3, NP4 and NP5 demonstrated similar but sharper dehydration peaks at 60–102 °C. The sharpness of the dehydration peaks and their shift to lower temperatures in Au-CS hNPs may be attributed to the possession of lower number of free NH_2 groups (that were used for reducing Au ions to metallic Au NPs) than CS that thereby facilitated the evaporation of the bound water molecules in the hybrid NPs. This finding was supported by the results reported in a previous study by Gadkari et al. [29]. Moreover, thermal decomposition of pure CS powder resulted in an exothermic peak at 322–337 °C. This peak appeared at 314–329, 322–342 and 322–345 °C for NP3, NP4 and NP5, respectively. Therefore, the decomposition of CS in NP4 and NP5 occurs at higher temperatures than NP3 indicating their thermal stability which may be due to the stronger interaction of CS with the formed metallic Au NPs. This shift of CSdecomposition peaks to higher temperatures agrees with the reported results in the literature [30].
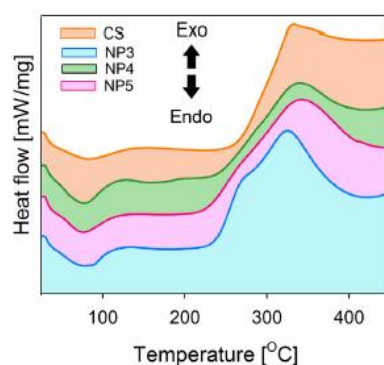
Fig. 6. Differential scanning calorimetry analysis of pure CS powder, NP3, NP4 and NP5. The DSC plots were recorded under N_2 atmosphere by applying a 10 °C/min heating rate.

3.6. Antimicrobial activity assessment

To determine the bactericidal potential of the synthesized Au-CS hNPs, S. aureus, P. aeruginosa and C. albicans were selected as the testing strains. The concentration of CS has clearly affected the antimicrobial activity of the as-prepared Au-CS hNPs. The biocidal effect was reduced for bigger hNPs prepared by using a CS concentration of 0.25 mg/mL (NP3). NP4 of median size (~25 nm) showed an intermediate antimicrobial effect. Meanwhile, the most effective antimicrobial hNPs found to be the NP5 which have the smallest size (~16.9 nm). The antimicrobial behavior of the developed hNPs can be proven by the lowest MIC value of NP5 in case of S. aureus, P. aeruginosa or C. albicans when compared to pure CS, NP3 and NP4.

As depicted by Fig. 7, the resistance of the tested microorganisms to CSandAu-CShNPsfollowstheorder:C.albicans>P.aeruginosa>S.aureus. Interestingly, NP5 showed the lowest MIC values in all of the three tested microorganisms, thereby it has the highest antimicrobial activity. In addition, CS showed the highest MIC values indicating that hybridization of CS with metallic Au NPs strongly enhanced its antimicrobial properties. The MIC values are in excellent agreement with the survival fractions of the microbes obtained from the CFU assay (Fig. 7(b–d)). Table 1 summarizes the physicochemical and antimicrobial properties of the investigated Au-CS hNPs. Although many attempts were carried out to explain the mechanism of microbial killing of Au-CS NPs, the mechanism is still unclear. Some researchers supposed that the interaction of CS cationic charges with the

Our findings are consistent with many other studies reporting that small-sized NPs can mediate much efficient antimicrobial activity than their large-sized counterparts [31,32]. It is expected that the high surface-to-volume ratio of the small-sized NPs is the reason beyond their good antimicrobial activity because of the more efficient exposure of the microbial cell walls to the NPs surface positive charges [32]. negatively charged microbial cell wall leads to the leakage of the intracellular components. Qi et al. (2004) and Orellano et al. (2019) reported that CS NPs lead to disruption of the microbial cell membranes and the leakage of cytoplasm [33,34].
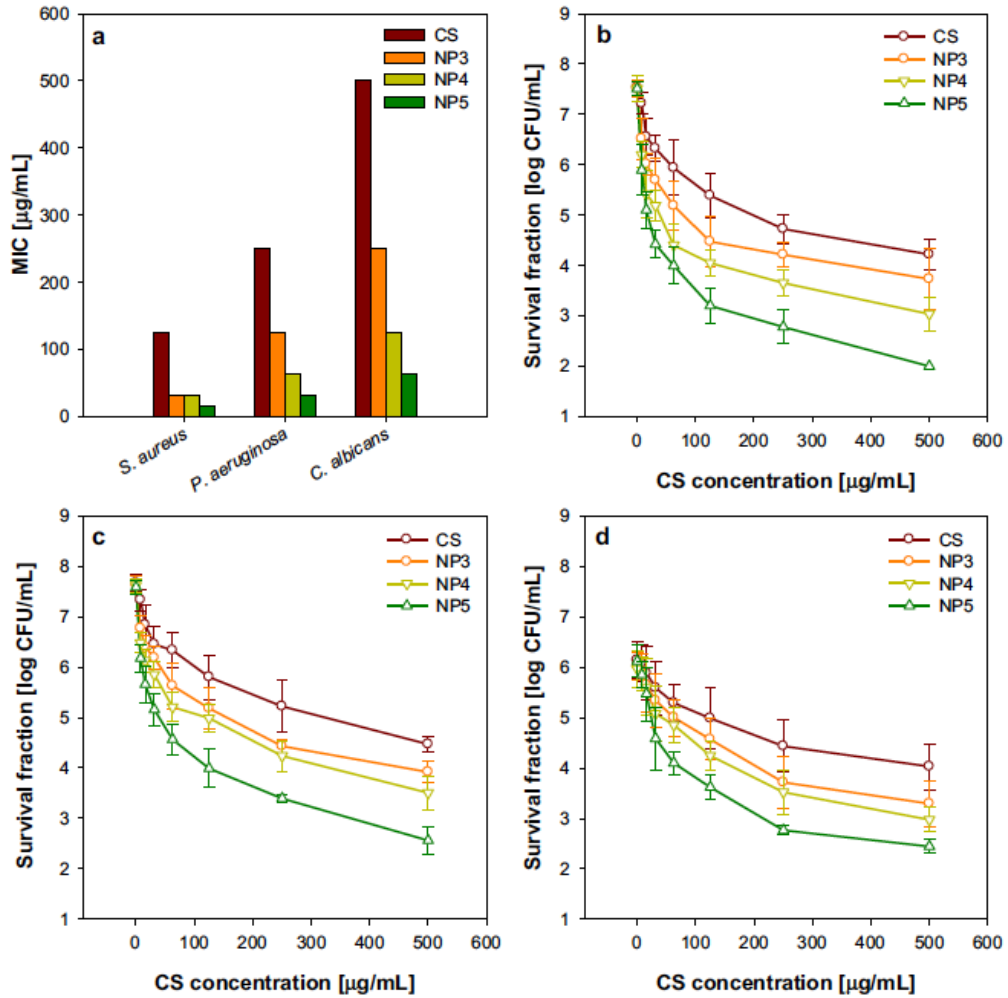
Fig. 7. MIC values (a) and CFU count assay of Au-CS hNPs prepared with different CS concentrations against *S. aureus* (b), *P. aeruginosa* (c) and *C. albicans* (d).

The thickness of the bacterial peptidoglycan layer plays a crucial role in the susceptibility of bacterial cell walls to CS-coated NPs. Some studies reported that the higher sensitivity of Gram positive bacteria may be attributed to their thinner peptidoglycan layer (7–8 nm) compared to that of the Gram negative bacteria (20–80 nm) [35]. Moreover, since Gram positive bacteria have multiple anionic binding sites on the outer surface of their cells walls (e.g. teichoic acid, phospholipids and cardiolipin) [36] than their Gram negative counterparts, they usually demonstrate higher sensitivity to CS-coated NPs. This fact agrees with the findings obtained in the present investigation where the Gram positive S. aureus showed a higher susceptibility to the prepared Au-CS hNPs than the Gram negative P. aeruginosa. In the current study, thanks to the higher CS concentration for increasing the positive charges of NP5 (+53.1 mV) which interacts more intensively than NP4 (+39.8 mV) and NP3 (+25.1 mV) with the microbial cell walls; thus induced better bactericidal/fungicidal activities. Such relationship between the amount of cationic charges and the biocidal activity has been demonstrated in the work reported by Mansilla et al. [37].

To confirm the role of bacterial cell surface charge, S. aureus mutants lacking one or more genes involved in teichoic acid biosynthesis were tested in a previous study. The gene deletion mutation associated with complete lack of teichoic acids from in cell wall (tagO, deletion mutant) displayed the highest resistance to chitosan (with more than fivefold higher MIC), followed by other mutants associated with partial lacking of teichoic acids.

Such findings confirm that less negatively charged cell wall, as a result of partial or complete absence of teichoic acids, could increase the resistance of S. aureus to chitosan [38]. In another study, S. aureus mutation associated with modification in teichoic acid with increasing its expression of negative charges, showed high susceptibility (100 times) to cationic antimicrobial agents [39].

Table 1
Physicochemical properties and antimicrobial activities of NP3, NP4 and NP5.

Au-CS hNPs		NP3	NP4	NP5
CS concentration[a] (µg/mL)		250	500	1000
Shape		Spherical	Spherical	Spherical
Size (nm) ± RSD	TEM-based	34.7 ± 7.6	25.4 ± 5.4	16.9 ± 3.9
	DLS-based	63.9 ± 21.1	46.1 ± 13.5	36.5 ± 11.5
ζ-potential (mV)		+25.1 ± 7.8	+39.8 ± 7.2	+53.1 ± 6.7
MIC[b] (µg/mL)	S. aureus	31.2	31.2	15.6
	P. aeruginosa	125	62.5	31.2
	C. albicans	250	125	62.5

[a] The concentration of CS used for the synthesis of Au-CS hNPs via reaction with 125 µmol/L AuHCl$_4$.
[b] The MIC of pure CS is 125, 250 and 500 µg/mL for S. aureus, P. aeruginosa and C. albicans, respectively.

Based on the above findings, we can claim that increasing the positive charges on the outer surface of Au NPs through increasing the concentration of the reductive chitosan permits more interaction of the NPs with the negatively charged surface components of many fungi and bacteria through electrostatic interaction causing significant cell surface alterations, leakage of intracellular substances, and ultimately resulting in the impairment of vital microbial activities specifically in Gram positive bacteria. The susceptibility of Gram positive S. aureus seemed to be lower than that of Gram negative organisms including Pseudomonas aeruginosa. For fungi, it was thought that CS-based NPs interact with the fungal membranes leading to a downregulation of the H$^+$ pump and thus inducing cell death. The investigated Au-CS hNPs showed a CS-concentration-dependent fungicidal activity against C. albicans (NP5 > NP4 > NP3). An acceptable explanation from the literature may be the greater ability of small-sized Au-CS hNPs to penetrate the fungal cell wall and interact with sulfur-containing membrane proteins and phosphorus-containing DNA nitrogenous bases. The observation that C. albicans showed lower sensitivity to the Au-CS hNPs than bacteria agrees with the study reported by Ramakritinan et al. [40].

4. Conclusion

The present study reported a green synthesis method for Au-CS hNPs with the aid of CS as a capping and reducing agent. To the best of our knowledge, the influence of CS amount on the antimicrobial and physicochemical properties of Au-CS hNPs by applying very low concentrations of CS was investigated herein for the first time. The major findings reveal that the size of Au-CS hNPs is inversely proportional to the amount of CS used in the preparation procedure. On the other hand, the positive ζ-potential increases by increasing the amount of CS. Moreover, increasing the amount of CS improves the antimicrobial activity of the synthesized Au-CS hNPs in terms of MIC and CFU assays because the antibacterial activity was attributed to the small size and the positive ζ-potential that were obtained with the highest CS concentration. Furthermore, Au-CS hNPs with the highest amount of CS demonstrated the best thermal stability. In addition, it was noticed from this study that using a high and optimum amount of CS enhances the shelf-life stability of Au-CS hNPs to 6 months. Although we shed the light on the anticipated mechanism of

formation of Au-CS hNPs herein, extensive research is needed to prove the formation of Au-CS complex prior to the chemical reduction of Au ions into metallic Au NPs. We are currently working on this aspect using more accurate analytical tools and computational chemistry.

Credit author author statement

- Mohamed A. Mohamady Hussein: Conceptualization, Methodology, Investigation, Visualization, Writing-Original draft, Funding acquisition.
- F. Guillermo Díaz Baños: Conceptualization, Resources, Funding acquisition.
- Mariusz Grinholc: Resources, Methodology, Funding acquisition.
- Ahmed S. Abo Dena: Methodology, Writing-Review and editing.
- Ibrahim M. El-Sherbiny: Methodology, Resources, Writing-Review and editing.
- Mosaad Megahed: Conceptualization, Methodology, Resources, Supervision, Project administration, Writing-Review and editing.

References

[1] R. Herizchi, E. Abbasi, M. Milani, A. Akbarzadeh, Current methods for synthesis of gold nanoparticles, Artif. Cells, Nanomedicine, Biotechnol. 44 (2016) 596–602, https://doi.org/10.3109/21691401.2014.971807.

[2] D. Cabuzu, A. Cirja, R.P., A.M. Grumezescu, Biomedical applications of gold nanoparticles, Curr. Top. Med. Chem. 15 (2015) 1605–1613, https://doi.org/10.2174/ 1568026615666150414144750.

[3] S. Pokhrel, P.N. Yadav, Functionalization of chitosan polymer and their applications, J. Macromol. Sci. Part A. 56 (2019) 450–475, https://doi.org/10.1080/10601325. 2019.1581576.

[4] D.I. Sánchez-Machado, J. López-Cervantes, M.A. Correa-Murrieta, R.G. SánchezDuarte, P. Cruz-Flores, G.S. de la Mora-López, Chapter 4.2 - chitosan, in: S.M. Nabavi, A.S. Silva (Eds.), Nonvitamin Nonmineral Nutr. Suppl, Academic Press 2019, pp. 485–493, https://doi.org/10.1016/B978-0-12-812491-8.00064-3.

[5] L. Zhao, Y. Wang, Z. Li, Y. Deng, X. Zhao, Y. Xia, Facile synthesis of chitosan-gold nanocomposite and its application for exclusively sensitive detection of Ag+ ions, Carbohydr. Polym. 226 (2019), 115290https://doi.org/10.1016/j.carbpol.2019. 115290.

[6] F.M. Reicha, A. Sarhan, M.I. Abdel-Hamid, I.M. El-Sherbiny, Preparation of silver nanoparticles in the presence of chitosan by electrochemical method, Carbohydr. Polym. 89 (2012) 236–244, https://doi.org/10.1016/j.carbpol.2012.03.002.

[7] S. Bonardd, C. Saldías, O. Ramírez, D. Radić, F.J. Recio, M. Urzúa, A. Leiva, A novel environmentally friendly method in solid phase for in situ synthesis of chitosan-gold bionanocomposites with catalytic applications, Carbohydr. Polym. 207 (2019) 533–541, https://doi.org/10.1016/j.carbpol.2018.12.009.

[8] K.B. Male, J. Li, C.C. Bun, S.-C. Ng, J.H.T. Luong, Synthesis and stability of fluorescent gold nanoparticles by sodium borohydride in the presence of mono-6-deoxy-6pyridinium-β-cyclodextrin chloride, J. Phys. Chem. C 112 (2008) 443–451, https:// doi.org/10.1021/jp7099515.

[9] A. Irure, M. Marradi, B. Arnáiz, N. Genicio, D. Padro, S. Penadés, Sugar/gadoliniumloaded gold nanoparticles for labelling and imaging cells by magnetic resonance imaging, Biomater. Sci. 1 (2013) 658–668, https://doi.org/10.1039/C3BM60032G.

[10] Y. Liu, S. Kim, Y.-J. Kim, H. Perumalsamy, S. Lee, E. Hwang, T.-H. Yi, Green synthesis of gold nanoparticles using Euphrasia officinalis leaf extract to inhibit lipopolysaccharide-induced inflammation through NF-κB and JAK/STAT pathways in RAW 264.7 macrophages, Int. J. Nanomedicine 14 (2019) 2945–2959, https:// doi.org/10.2147/IJN.S199781.

[11] M. Sharon, A. Mewada, N. Swaminathan, C. Sharon, Synthesis of Biogenic Gold Nanoparticles and its Applications as Theranostic Agent: A Review, 2017 1.

[12] D.R. Bhumkar, H.M. Joshi, M. Sastry, V.B. Pokharkar, Chitosan reduced gold nanoparticles as novel carriers for transmucosal delivery of insulin, Pharm. Res. 24 (2007) 1415–1426, https://doi.org/10.1007/s11095-007-9257-9.

[13] R. Sharma, R. Raghav, K. Priyanka, P. Rishi, S. Sharma, Exploiting Chitosan and Gold Nanoparticles for Antimycobacterial Activity of In Silico Identified Antimicrobial Motif of Human Neutrophil Peptide-1, 2019 1–14, https://doi.org/10.1038/s41598019-44256-6.

[14] X. Guo, Q. Zhuang, T. Ji, Y. Zhang, C. Li, Y. Wang, H. Li, H. Jia, Y. Liu, L. Du, Multifunctionalized chitosan nanoparticles for enhanced chemotherapy in lung cancer, Carbohydr. Polym. 195 (2018) 311–320, https://doi.org/10.1016/j.carbpol.2018.04. 087.

[15] C.O. Mohan, S. Gunasekaran, C.N. Ravishankar, Chitosan-capped gold nanoparticles for indicating temperature abuse in frozen stored products, Npj Sci. Food. 3 (2019) 1–6, https://doi.org/10.1038/s41538-019-0034-z.

[16] A.L. Barry, R.A. Lasner, In-vitro methods for determining minimal lethal concentrations of antimicrobial agents, Am. J. Clin. Pathol. 71 (1979) 88–92, https://doi.org/ 10.1093/ajcp/71.1.88.

[17] G. Fila, A. Kawiak, M. Grinholc, Blue light treatment of Pseudomonas aeruginosa: strong bactericidal activity, synergism with antibiotics and inactivation of virulence factors, Virulence. 8 (0) (2016)https://doi.org/10.1080/21505594.2016.1250995.

[18] P.U. Londhe, M. More, N.B. Chaure, Influence of capping agents on the growth of gold nanoparticles from aqueous and non-aqueous medium, Int. Conf. Adv. Nanomater. Emerg. Eng. Technol 2013, pp. 317–319, https://doi.org/10.1109/ ICANMEET.2013.6609301.

[19] R. Tamrakar, M. Ramrakhiani, B.P. Chandra, Effect of capping agent concentration on photophysical properties of zinc sulfide nanocrystals, Open Nanosci. J. 2 (2008) 12–16, https://doi.org/10.2174/1874140100802010012.

[20] T. Zhang, M. Dang, W. Zhang, X. Lin, Gold nanoparticles synthesized from Euphorbia fischeriana root by green route method alleviates the isoprenaline hydrochloride induced myocardial infarction in rats, J. Photochem. Photobiol. B Biol. 202 (2020) 111705, https://doi.org/10.1016/j.jphotobiol.2019.111705.

[21] B. Ajitha, Y.A. Kumar Reddy, P.S. Reddy, H.J. Jeon, C.W. Ahn, Role of capping agents in controlling silver nanoparticles size, antibacterial activity and potential application as optical hydrogen peroxide sensor, RSC Adv. 6 (2016) 36171–36179, https://doi. org/10.1039/c6ra03766f.

[22] F. Faghihzadeh, N.M. Anaya, L.A. Schifman, V. Oyanedel-Craver, Fourier transform infrared spectroscopy to assess molecular-level changes in microorganisms exposed to nanoparticles, Nanotechnol. Environ. Eng. 1 (1) (2016)https://doi.org/10.1007/ s41204-016-0001-8.

[23] J. Kiefer, J. Grabow, H.-D. Kurland, F.A. Müller, Characterization of nanoparticles by solvent infrared spectroscopy, Anal. Chem. 87 (2015) 12313–12317, https://doi. org/10.1021/acs.analchem.5b03625.

[24] P. Abrica-González, J.A. Zamora-Justo, A. Sotelo-López, G.R. Vázquez-Martínez, J.A. Balderas-López, A. Muñoz-Diosdado, M. Ibáñez-Hernández, Gold nanoparticles with chitosan, N-acylated chitosan, and chitosan oligosaccharide as DNA carriers, Nanoscale Res. Lett. 14 (2019)https://doi.org/10.1186/s11671-019-3083-y.

[25] L.S. Wang, C.Y. Wang, C.H. Yang, C.L. Hsieh, S.Y. Chen, C.Y. Shen, J.J. Wang, K.S. Huang, Synthesis and anti-fungal effect of silver nanoparticles–chitosan composite particles, Int. J. Nanomedicine 10 (2015) 2685–2696, https://doi.org/10.2147/IJN.S77410.

[26] M. Mollick, B. Bhowmick, D. Mondal, D. Maity, D. Rana, S. Dash, S. Chattopadhyay, S. Roy, J. Sarkar, K. Acharya, M. Chakraborty, D. Chattopadhyay, Anticancer (in vitro) and antimicrobial effect of gold nanoparticles synthesized using Abelmoschus esculentus (L.) pulp extract via green route, RSC Adv. 4 (2014) 37838–37848, https://doi.org/10.1039/C4RA07285E.

[27] S. Ahn, P. Singh, M. Jang, Y.J. Kim, V. Castro-Aceituno, S.Y. Simu, Y.J. Kim, D.C. Yang, Gold nanoflowers synthesized using Acanthopanacis cortex extract inhibit inflammatory mediators in LPS-induced RAW264.7 macrophages via NF-κB and AP-1 pathways, Colloids Surfaces B Biointerfaces 162 (2018) 398–404, https://doi.org/ 10.1016/j.colsurfb.2017.11.037.

[28] A. Sungeun, P. Singh, M. Jang, Y.-J. Kim, V. Castro-Aceituno, S. Simu, Y.-J. Kim, D.-C. Yang, Gold nanoflowers synthesized using Acanthopanacis cortex extract inhibit inflammatory mediators in LPS-induced RAW264.7 macrophages via NF-κB and AP-1 pathways, Colloids Surfaces B Biointerfaces 160 (2017)https://doi.org/10.1016/j. colsurfb.2017.09.053.

[29] R.R. Gadkari, S. Suwalka, M.R. Yogi, W. Ali, A. Das, R. Alagirusamy, Green synthesis of chitosan-cinnamaldehyde cross-linked nanoparticles: characterization and antibacterial activity, Carbohydr. Polym. 226 (2019), 115298https://doi.org/10.1016/j. carbpol.2019.115298.

[30] C. Sámano-valencia, G.A. Martínez-castañón, R.E. Martínez-martínez, Bactericide Efficiency of a Combination of Chitosan Gel with Silver Nanoparticles, vol. 106, 2013 413–416, https://doi.org/10.1016/j.matlet.2013.05.075.

[31] S. Agnihotri, S. Mukherji, S. Mukherji, Size-controlled silver nanoparticles synthesized over the range 5–100 nm using the same protocol and their antibacterial efficacy, RSC Adv. 4 (2014) 3974–3983, https://doi.org/10.1039/C3RA44507K.

[32] M.A. Raza, Z. Kanwal, A. Rauf, A.N. Sabri, S. Riaz, Size- and Shape-Dependent Antibacterial Studies of Silver Nanoparticles Synthesized by Wet Chemical Routes, (n. d.). doi:https://doi.org/10.3390/nano6040074.

[33] L. Qi, Z. Xu, X. Jiang, C. Hu, X. Zou, Preparation and antibacterial activity of chitosan nanoparticles, Carbohydr. Res. 339 (2004) 2693–2700, https://doi.org/10.1016/j. carres.2004.09.007.

[34] M.S. Orellano, P. Isaac, M.L. Breser, L.P. Bohl, A. Conesa, R.D. Falcone, C. Porporatto, Chitosan nanoparticles enhance the antibacterial activity of the native polymer against bovine mastitis pathogens, Carbohydr. Polym. 213 (2019) 1–9, https://doi. org/10.1016/j.carbpol.2019.02.016.

[35] P. Eaton, J.C. Fernandes, E. Pereira, M.E. Pintado, F. Xavier Malcata, Atomic force microscopy study of the antibacterial effects of chitosans on Escherichia coli and Staphylococcus aureus, Ultramicroscopy 108 (2008) 1128–1134, https://doi.org/10.1016/ j.ultramic.2008.04.015.

[36] M.A. Matica, F.L. Aachmann, A. Tøndervik, H. Sletta, V. Ostafe, Chitosan as a wound dressing starting material: antimicrobial properties and mode of action, Int. J. Mol. Sci. 20 (2019) 5889, https://doi.org/10.3390/ijms20235889.

[37] A.Y. Mansilla, L. Albertengo, M.S. Rodríguez, A. Debbaudt, A. Zúñiga, C.A. Casalongué, Evidence on antimicrobial properties and mode of action of a chitosan obtained from crustacean exoskeletons on Pseudomonas syringae pv. tomato DC3000, Appl. Microbiol. Biotechnol. 97 (2013) 6957–6966, https://doi.org/10.1007/s00253-0134993-8.

[38] D. Raafat, K. von Bargen, A. Haas, H.-G. Sahl, Insights into the mode of action of chitosan as an antibacterial compound, Appl. Environ. Microbiol. 74 (2008) 3764–3773, https://doi.org/10.1128/AEM.00453-08.

[39] A. Peschel, M. Otto, R.W. Jack, H. Kalbacher, Inactivation of the dlt Operon in Staphylococcus aureus Confers Sensitivity to Defensins, Protegrins, and Other Antimicrobial Peptides *, vol. 274, 1999 8405–8410.

[40] R. Kalaivani, M. Maruthupandy, T. Muneeswaran, M. Singh, S. Sureshkumar, M. Anand, C.M. Ramakritinan, F. Quero, A.K. Kumaraguru, Chitosan mediated gold nanoparticles against pathogenic bacteria, fungal strains and MCF-7 cancer cells, Int. J. Biol. Macromol. 146 (2020) 560–568, https://doi.org/10.1016/j.ijbiomac. 2020.01.037.